LIMNOLOGY and OCEANOGRAPHY

ASLO

Limnol. Oceanogr. 66, 2021, 3134–3148

doi: 10.1002/lno.11866

Plankton respiration in the Atacama Trench region: Implications for particulate organic carbon flux into the hadal realm

Igor Fernández-Urruzola [1]*, Osvaldo Ulloa [1,2], Ronnie N. Glud [3,4,5], Matthew H. Pinkerton [6], Wolfgang Schneider [1,2], Frank Wenzhöfer [3,7,8], Rubén Escribano [1,2]

[1]Millennium Institute of Oceanography, Universidad de Concepción, Concepción, Chile
[2]Department of Oceanography, Universidad de Concepción, Concepción, Chile
[3]HADAL & Nordcee, Department of Biology, University of Southern Denmark, Odense, Denmark
[4]Danish Institute for Advanced Study, University of Southern Denmark, Odense, Denmark
[5]Department of Ocean and Environmental Sciences, Tokyo University of Marine Science and Technology, Tokyo, Japan
[6]National Institute of Water & Atmospheric Research Ltd, Wellington, New Zealand
[7]Alfred Wegener Institute, Helmholtz Center for Polar and Marine Research, Bremerhaven, Germany
[8]Max Planck Institute for Marine Microbiology and Ecology, Bremen, Germany

Abstract

Respiration is a key process in the cycling of particulate matter and, therefore, an important control mechanism of carbon export to the ocean's interior. Most of the fixed carbon is lost in the upper ocean, and only a minor amount of organic material sustains life in the deep-sea. Conditions are particularly extreme in hadal trenches, and yet they host active biological communities. The source of organic carbon that supports them and the contribution of these communities to the ocean carbon cycle, however, remain uncertain. Here we report on size-fractionated depth profiles of plankton respiration assessed from the activity of the electron transport system in the Atacama Trench region, and provide estimates of the minimum carbon flux (*FC*) needed to sustain the respiratory requirements from the ocean surface to hadal waters of the trench and shallower nearby sites. Plankton < 100 μm contributed about 90% to total community respiration, whose magnitude was highly correlated with surface productivity. Remineralization rates were highest in the euphotic zone and declined sharply within intermediate oxygen-depleted waters, remaining fairly constant toward the bottom. Integrated respiration in ultra-deep waters (> 1000 m) was comparable to that found in upper layers, with 1.3 ± 0.4 mmol C m^{-2} d^{-1} being respired in the hadopelagic. The comparison between our *FC* models and estimates of sinking particle flux revealed a carbon imbalance through the mesopelagic that was paradoxically reduced at greater depths. We argue that large fast-sinking particles originated in the overlying surface ocean may effectively sustain the respiratory carbon demands in this ultra-deep marine environment.

The deep ocean covers most of our planet, yet it is among the least understood biomes on Earth. It is, in many ways, an inhospitable environment where the absence of light, low temperatures and high hydrostatic pressures restrict life to specialized biota. Conditions are particularly extreme in the lower-abyssal and hadal waters of marine trenches, which represent the most remote and unexplored regions of the world oceans (Jamieson 2018). Continuous technological advances in the last decades have made these challenging ecosystems more accessible, and there are now increasing evidence that these are surprisingly complex and dynamic habitats with diverse pelagic communities and active metabolic life (e.g., Blankenship et al. 2006; Nunoura et al. 2015). Life that requires energy for sustenance.

Autochthonous photosynthetic production is absent in the deep ocean and dark carbon fixation through chemosynthesis accounts for only a marginal proportion of the total carbon supply in non-vent habitats (Tyler 2003). Life at depth thus relies upon the input of organic material sinking down from the sunlit surface ocean. Such dependency on surface processes highlights the need to look at the upper water column dynamics, which are characterized by intense feedback loops between production and consumption, to better understand the ecological functioning of the deep pelagic realm. Highly

*Correspondence: igor.fernandez@imo-chile.cl

Additional Supporting Information may be found in the online version of this article.

productive epipelagic waters usually result in substantial transport of biogenic material from the illuminated layer to the ocean interior (Buesseler 1998) and therefore, these are expected to meet greater metabolic demands at depth than more oligotrophic surface waters. Not surprisingly, hadal trenches underlying productive regions, such as the Atacama Trench, contain high faunal densities compared to trenches with predictably lower inputs of particulate material (Danovaro et al. 2002; Fujii et al. 2013; Leduc et al. 2016).

The amount of organic carbon reaching the deep-sea, however, is ultimately constrained by the efficiency of the biological pump. Key to its effectiveness is the magnitude of carbon fluxing out of the euphotic zone (Buesseler et al. 2020) and the remineralization depth of the sinking material (Marsay et al. 2015). Most of the fixed carbon is lost from the organic pool via respiration as it falls through the water column, and less than 2% of the carbon exported from the surface is estimated to eventually deposit at the deep-sea sediment surface (De La Rocha and Passow 2007). Despite the difficulties in reconciling the carbon budget, with deep-ocean respiration typically exceeding the carbon supply (e.g., Baltar et al. 2009), both carbon flux attenuation and community respiration should, in theory, be balanced at steady-state conditions (Giering et al. 2014). Given the reciprocal relationship between the two processes, they could be then derived from each other. Based on this premise, Suess (1980) predicted remineralization rates from the first derivative of the decay of organic matter below the euphotic zone. The same rationale in reverse was applied by Packard et al. (2015) to model particulate organic carbon (POC) flux (*FC*) from respiratory CO_2 production. Here, we use this latter approach to build *FC* profiles throughout the entire water column at two sites in the Atacama Trench and four nearby reference sites to evaluate the respiratory carbon needs of a pelagic community in one of the world's deepest ecosystems.

The dark ocean is sensitive to ongoing climatic and anthropogenic changes (Levin and Bris 2015), making it critical to establish reliable baselines to explore system responses in the deep-sea. Predicted changes in the primary production and increased stratification will impact the organic carbon exported to great depths, with direct implications for deep ocean ecosystem processes such as respiration (Smith et al. 2008). This research work aims to provide the first insights into the minimum carbon supply required to sustain the respiratory demands down to the hadopelagic zone of the Atacama Trench and into the relative contribution of the two main components of the plankton community (i.e., plankton < 100 μm and mesozooplankton) to carbon remineralization throughout this water column and shallower adjacent sites. We further address possible imbalances in the pelagic carbon cycle by a direct comparison between our respiratory *FC* and alternative estimates of gravitational carbon flux in the region.

Methods

Study site and sampling

Samples were collected during the austral summer 2018 (from 02 February to 21 March) off the northern Chilean coast (Fig. 1A) onboard the Chilean RV Cabo de Hornos (LowpHox II cruise) and the German RV *Sonne* (So261 cruise). Stations were located at the continental shelf (Sites A1, T3, and T5), in

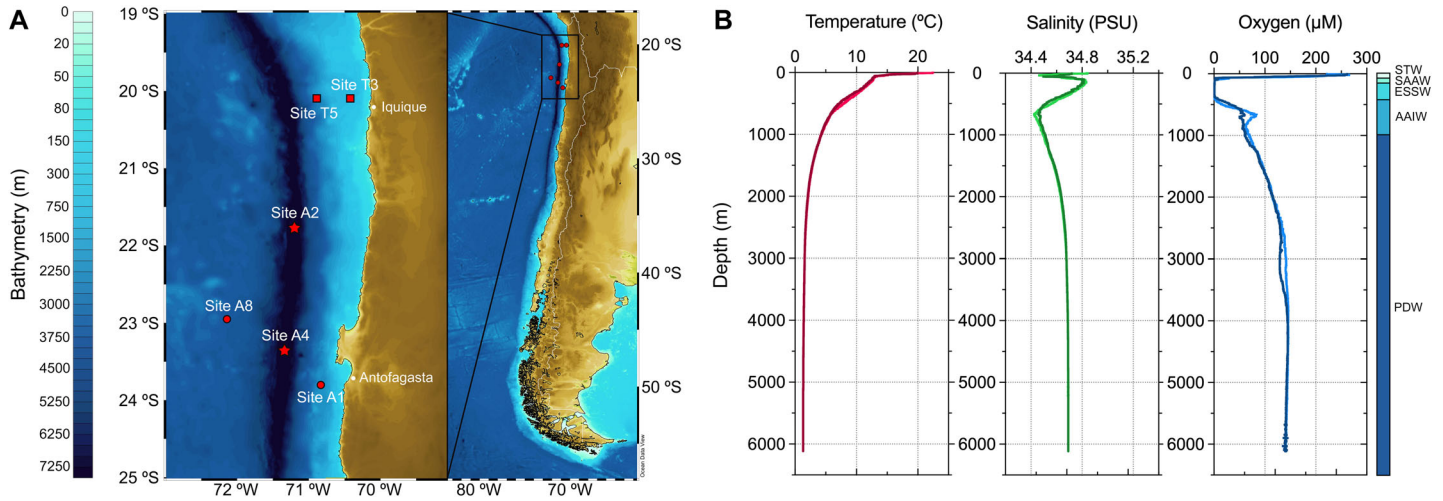

Fig 1. (**A**) Stations sampled during the LowpHox II and So261 cruises in the austral summer 2018. Star symbols stand for those stations where ultradeep biological samples were taken. Squares and stars indicate stations sampled for both zooplankton and plankton < 100 μm, whereas circles indicate stations sampled only for plankton < 100 μm. (**B**) Temperature, salinity and oxygen depth-profiles in Sites A2 and A4 over the Atacama trench, both depicting the typical profiles in the region with five water bodies well-differentiated throughout the water column (right color bar): subtropical water (STW), subantarctic water (SAAW), equatorial subsurface water (ESSW), Antarctic intermediate water (AAIW), and the Pacific deep water (PDW). Note the characteristic hypoxic core of the OMZ between 90 and 450 m.

the transition zone over the Atacama Trench (Sites A4 and A2) and farther offshore (Site A8). Hydrographic data above 6000 m were obtained at all stations by deployment of a Seabird SBE-9 plus CTD equipped with an oxygen sensor and mounted on a rosette sampler with 24 10-L Niskin bottles. Water samples between 6000 and 7000 m were collected using a custom-build autonomous "hadal rosette" equipped with 8 10-L Niskin bottles.

Once on deck, the Niskin bottles were drained, with a prefiltration through 100 μm nylon mesh, into well-rinsed carboys. Seawater (volume ranging from ~ 0.5 to 60 L depending on the depth) from several discrete depths of the water column was gently filtered through Whatman GF/F filters for the electron transport system (ETS) activity in plankton < 100 μm, as explained below. Although this size fraction includes all organisms within the 0.7–100 μm size range, it will be dominated by bacteria and ciliate protozoa. Filters were immediately snap-frozen in liquid N until analyses. In parallel, similar volumes of seawater at selected depths were filtered onto precombusted (450°C, 24 h) GF/F filters for analysis of total organic carbon.

Zooplankton samples were also collected in most stations (Sites A2, A4, T3, and T5). Zooplankton from the uppermost 1000 m of the water column was gathered at five depth strata by vertical hauls of a Multinet (Hydro-Bios) with 0.25 m^2 openings and 333 μm mesh nets. A flowmeter mounted in the net frame quantified the volume of water filtered at each haul. The five depth strata sampled by the Multinet (0–30 m, 30–90 m, 90–150 m, 150–400 m, 400–800 m) were set on the basis of the different water bodies that occupy the water column (Fig. 1B). Zooplankton from depths between 1000 and 5000 m was sampled every 1000 m using a MOCNESS net system (10 m^2 mouth opening with 333 μm mesh aperture netting), equipped with conductivity, pressure, oxygen and temperature sensors, as well as with a flowmeter. Both Multinet and MOCNESS net hauls were always performed consecutively between dusk and dawn. Zooplankton samples were gently subsampled with a Motoda splitter, and subsamples stored at − 80°C after snap-freezing in liquid N for enzymatic analyses. Prior to preservation, the subsamples were fractionated for the 333–500 μm, 500–1000 μm, 1000–2000 μm, 2000–5000 μm size classes.

ETS activity as an index of respiration

Respiratory ETS activity was measured in all samples as a proxy for respiration. The ETS activity in plankton < 100 μm was assayed by measuring the reduction of the electron transport acceptor INT into INT-formazan after Kenner and Ahmed (1975). All ETS activities were corrected to in situ temperatures using the Arrhenius equation following Packard et al. (1975). The rate of formazan production was then stoichiometrically related to oxygen consumption as explained in Maldonado et al. (2012) and converted into actual respiration (RO_2) by applying a R/ETS factor of 0.58, which was empirically determined in microplankton communities from similar upwelling ecosystems (Arístegui and Montero 1995). In oxygen deficient waters, NO_x^- may replace O_2 as the terminal electron acceptor, so the calculations required an alternative redox stoichiometry (*see* Table S1).

A similar analytical procedure was performed to measure the ETS activity in zooplankton samples, with some modifications according to Owens and King (1975). The specific R/ETS ratio used to calculate zooplankton respiration (0.48) was previously obtained in a comparable mesozooplankton community (Fernández-Urruzola et al. 2014).

Protein content was also analyzed in all homogenates as a straightforward proxy for biomass. Analyses were done by triplicate following the modified Lowry-SDS method (Cadman et al. 1979). Bovine serum albumin was used as a standard for the calibration curves.

***F*C calculations from RO_2 depth profiles**

The RO_2 assessed throughout the water column served to generate vertical *F*C models down to the bottom following the rationale described by Osma et al. (2014). Respiration data were first recalculated into carbon units using a revised molar Redfield ratio (C/O_2) of 0.71 (Takahashi et al. 1985) and then, fitted to a power function in the form of:

$$(R\mathrm{CO}_2)_z = (R\mathrm{CO}_2)_m \, (z/z_m)^{-b} \quad (1)$$

where $(R\mathrm{CO}_2)_z$ is the respiration at a given depth, $(R\mathrm{CO}_2)_m$ is the maximum respiration in the water column, z_m is the depth where $(R\mathrm{CO}_2)_m$ was measured and z is depth. The exponent b describes the function's curvature, thus being a key parameter in determining the carbon flux attenuation. Assuming that respiration is the primary mechanism for carbon remineralization through the water column, both $R\mathrm{CO}_2$ and *F*C can be mathematically related as a continuous function of depth as follows:

$$\int_{z1}^{z2} R\mathrm{CO}_2 \, \mathrm{d}z = \mathrm{FC}z_1 - \mathrm{FC}z_2 \quad (2)$$

In other words, the integrated respiration in an ocean layer represents the difference between the carbon flux (FC_{z1}) entering such layer at depth z_1 and the carbon flux (FC_{z2}) leaving the layer at depth z_2. This concept may be extrapolated to calculate the *F*C required at any depth (FC_z) below the euphotic zone (z_e), defined as the depth where the photosynthetic available radiation (PAR) is 1% of its surface value, to meet the heterotrophic carbon demands from that depth (z) to the seafloor (z_s), as expressed in Eq. 3:

$$\begin{aligned} FC_z &= \int_z^{zs} (R\mathrm{CO}_2)_m \, (z/z_m)^{-b} \, \mathrm{d}z \\ &= \left\{ (R\mathrm{CO}_2)_m / \left[(-b+1) \, {z_m}^{-b} \right] \right\} \left({z_s}^{-b+1} - z^{-b+1} \right) \end{aligned} \quad (3)$$

Accordingly, the respiratory carbon needs for specific vertical zones can be determined by simply setting the upper and lower depth limits of the integral. This allowed us to estimate the carbon losses occurring in the epipelagic (z_e–150 m), mesopelagic (150–1000 m), bathypelagic (1000–4000 m), abyssopelagic (4000–6000 m) and hadopelagic (> 6000 m) realms.

POC flux estimates

For comparison with the respiratory *F*C profiles, we modeled the passive POC flux from various approaches: (1) First, we fitted a Martin curve (Martin et al. 1987) to sedimentation rates of POC measured by free-drifting sediment traps at four different depths (65, 100, 200, and 300 m) both in the coastal and oceanic areas at 23°S off Antofagasta (data published in González et al. 1998). (2) We then used the model of Lutz et al. (2002), which applies empirical estimates of export fraction and flux attenuation with depth to mixed-layer net primary productivity (NPP) values based on satellite observations. (3) A third model, the GBC14 global export model of Siegel et al. (2014), was also provided. This food-web based method is based on satellite measurements of particulate backscatter, phytoplankton biomass, primary productivity, z_e depth and mixed layer depth. Attenuation of export flux with depth was based on a power-law function (Eq. 4) where POC flux_z is the flux at depth z, POC flux_{100} is the export flux (nominally at 100 m depth), and b is the attenuation exponent. A range of b-values (0.36–1.33, $\bar{x} = 0.78$) were considered to explore the effect of uncertainties in flux attenuation on POC flux at depth. Two versions of the Lutz and GBC14 models were calculated: one based on the Carbon-based Production Model (CbPM) to estimate phytoplankton biomass (Westberry et al. 2008), and another based on NPP estimated from the Vertically Generalized Production Model (VGPM) developed by Behrenfeld and Falkowski (1997), sourced from Oregon State University "Ocean Productivity" project (www.science.oregonstate.edu/ocean.productivity). Detailed information about parametrization and the satellite-based products used for the POC flux estimates can be found in the Supplementary Information.

$$\text{POC flux}_z = \text{POC flux}_{100}\,(z/100)^{-b} \quad (4)$$

Statistical analyses

Nonlinear least squares curve fitting was performed using GraphPad Prism (v8.4, GraphPad), which uses an adapted version of the Marquardt nonlinear regression algorithm. The goodness of fit was expressed as the 95% confident limits on the parameter values. The best fit for both the RCO_2 data and the *F*C data was chosen according to the Akaike's information criterion (AIC_c). A propagation of errors was additionally performed using a Monte Carlo approach to assess the uncertainties on the final models. Either parametric or nonparametric tests were applied to test significant differences in the values and model parameters between zones, once the normality and homoscedasticity of residuals were confirmed through Kolmogorov–Smirnov and Levene's tests, respectively.

Results

Hydrography

There was a strong gradient in the oceanographic features with depth in all stations, especially within the upper 1000 m. Temperature decreased consistently across the water column, with shallow thermoclines at ~ 30 m (Fig. 1B). Salinity followed a different pattern, as it increased between ~ 25 and 70 m associated with the Equatorial Subsurface Waters (ESSW), coinciding with the characteristically shallow oxygen minimum zone (OMZ). These oxygen-deficient waters generally extended down to 500 m, with a hypoxic core (< 4.5 μM O_2) between ~ 90 and 450 m. Hydrographic and productive conditions at the time of sampling are also described in

Table 1. Hydrographic characterization of those stations sampled for the study located on the continental slope (C.S.), the Atacama Trench (A.T.) and the abyssal plain (A.P.) off northern Chile. SST and NPP stand for the sea surface temperature and net primary production, respectively. NPP estimations are derived from remote sensing data and the VGPM. The oxygen minimum zone (OMZ) considers seawater with a dissolved oxygen concentration below 9 μM. Measured particulate organic carbon (POC) concentrations at 5, 1000, and 7000 m are also presented (*n.d.* stands for no-data).

Sta.	Location	Seafloor (m)	Sampling date (2018)	z_e (m)	OMZ* (m)	SST (°C)	NPP (mmol C m^{-2} d^{-1})	$POC_{5\ m}$ (μM)	$POC_{1000\ m}$ (μM)	$POC_{7000\ m}$ (μM)
Site T3	C.S.	1090	05 Feb	21	26	21.1	259.5	19.0	n.d.	–
Site T5	C.S.	2890	04 Feb	37	52	24.8	48.1	5.3	n.d.	–
Site A1	C.S.	2560	05 Mar	29	82	20.2	157.8	5.9	1.0	–
Site A2	A.T.	7995	25 Mar	40	69	19.9	132.6	8.1	1.4	1.1
Site A4	A.T.	8085	14 Mar	27	94	22.4	62.7	5.5	1.2	1.0
Site A8	A.P.	4000	21 Mar	34	68	20.4	56.9	5.0	n.d.	–

*Upper boundary depth of the OMZ.

Table 1. In general, the coastal stations situated over the slope (Sites T3 and A1) presented colder sea surface temperatures and higher productivities. On the contrary, the offshore station Site A8 was much less productive (56.9 mmol C m^{-2} d^{-1}). These differences in the productivity were also reflected in the POC concentration at surface, which was notably higher at the shallower Site T3 (19.0 μM) compared to the other stations. This had implications for the z_e depth, which decreases with increasing amounts of particles in the seawater.

Plankton biomass and respiration depth-profiles

Measured ETS-based respiration rates in plankton < 100 μm (Fig. 2) showed a step decrease with depth in all stations. Highest rates were always found above the OMZ, with maximum surface values ranging from 1246.3 μmol C m^{-3} d^{-1} at Site T3 to 252.1 μmol C m^{-3} d^{-1} at the more oligotrophic Site A8. The protein content in plankton < 100 μm followed similar trends to those of respiration. Particularly low biomass-specific respiration rates were found at Site A8, where the plankton < 100 μm biomass throughout the water column was higher than in any other site. On the other hand, neither the respiration rates nor the protein values measured in the hadopelagic waters (averaging 13.5 ± 9.0 μmol C m^{-3} d^{-1} and 4.1 ± 0.7 mg protein m^{-3}, respectively) differed significantly from those values presented by the bathypelagic community (Student's *t*-test, *p*-value > 0.05 in both cases).

Similar depth-profiles were also generated for the zooplankton community, which followed the same general pattern with depth (Fig. 3). Nevertheless, the zooplankton biomass and respiration values were about an order of magnitude lower than those of plankton < 100 μm. Zooplankton biomass and respiration peaked in all cases within the upper 30 m to then decrease dramatically below 90 m, coinciding with the core of the OMZ (Fig. 3). This RCO_2 attenuation in the upper ocean was more pronounced than the corresponding one in plankton < 100 μm, as evidenced by the more negative *b*-values in the zooplankton RCO_2 power functions (Table S2). Again, the RCO_2 values measured in the upper layer were closely related to the estimated NPP in the epipelagic, reaching their maximum at Site T3 (where 30.1 mg protein m^{-3} of zooplankton respired 625.0 μmol C m^{-3} d^{-1}). Overall, the largest size class dominated the community biomass across the water column but, given that protein-specific RCO_2 was consistently higher in the smaller organisms (Fig. 3C), the relative contribution to total respiration was comparable between all sizes. The biomass-specific RCO_2 generally decreased with depth, from community averaged values of > 0.5 μmol C mg $protein^{-1}$ h^{-1} in the surface waters to < 0.2 μmol C mg $protein^{-1}$ h^{-1} below 150 m. An exception was found within the 90–150 m depth range (upper hypoxic layer), where the specific rates peaked in all cases. The combination of low biomass and low protein-specific RCO_2 resulted in very low volumetric RCO_2 at depth, especially for the smallest size class.

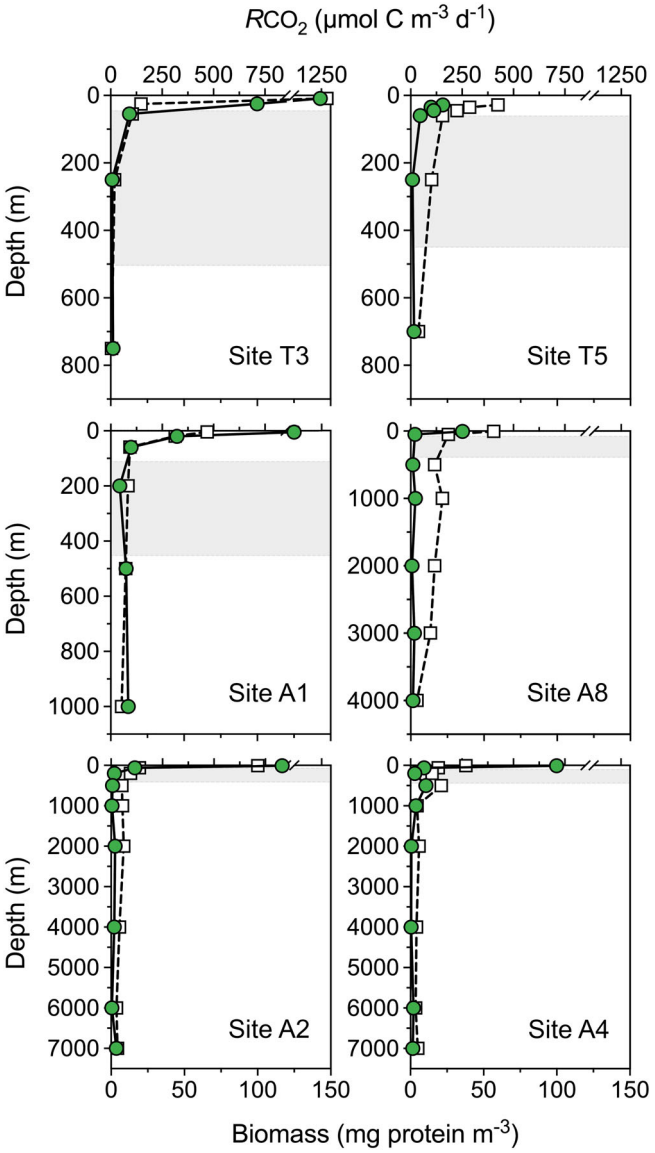

Fig 2. Respiration (green circles, upper *x*-axis) and biomass in terms of protein (white squares, lower *x*-axis) of the plankton community (< 100 μm) at each station. The hypoxic core of the OMZ (< 4.5 μM O_2), where denitrification processes dominate (Ulloa et al. 2012), is delimited in gray.

***F*C and size-fractionated respiratory carbon demand**

The vertical profiles of plankton respiration were used to model the minimum carbon flux (*F*C) needed throughout the whole water column to sustain the measured respiratory carbon demands. All calculations are detailed in Tables S1–S3. The selection of the best explanatory *F*C models (Fig. 4A) was based on the corrected Akaike's information criterion (AIC_c, *see* Table S4). The models were highly significant in all cases (-Tables S3, S4). In general, the *F*C associated with the plankton < 100 μm requirements followed a logarithmic decay with

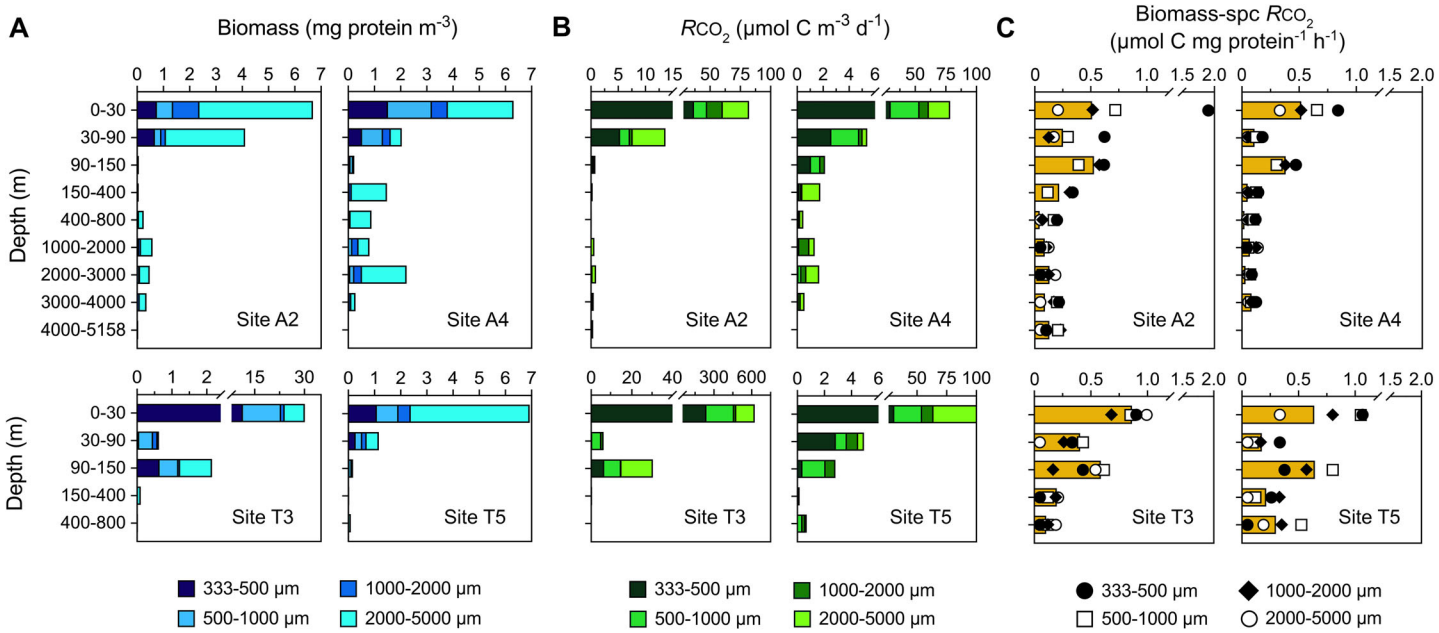

Fig 3. (**A**) Protein content and (**B**) respiration rates of each zooplankton size class across depth strata in those stations where plankton nets were deployed. (**C**) Protein-specific respiration rates, with yellow bars standing for the mean specific rates and symbols representing the individual rates of the corresponding size fractions. Note the changes in *x*-axis scales for Site T3.

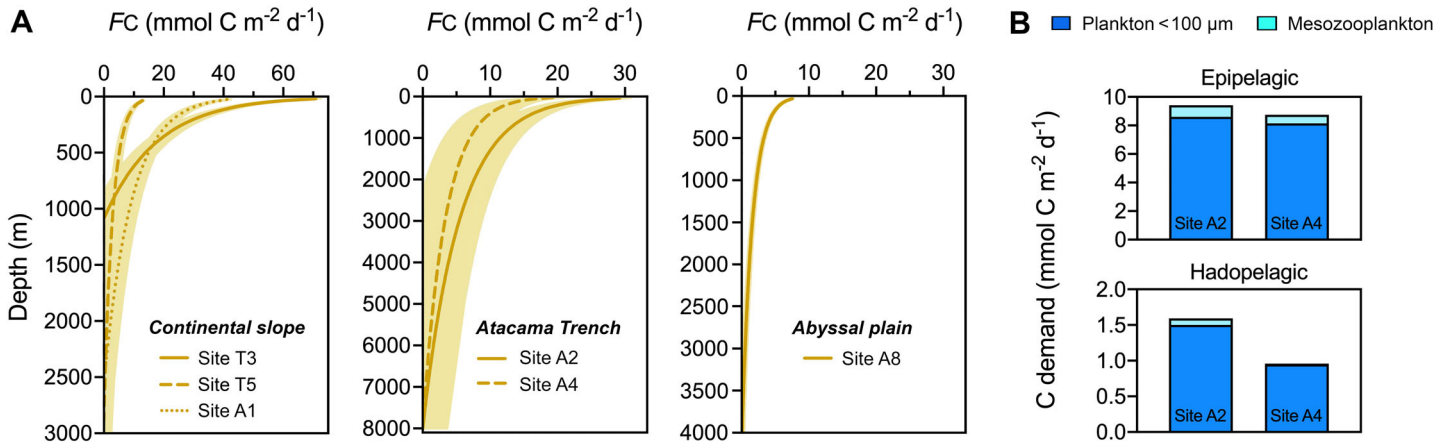

Fig 4. (**A**) *FC* profiles at those stations located over the continental slope, Atacama trench and abyssal plain off the northern Chilean coast. All equations and goodness of fits are given in Table S3. Light yellow represents the 95% profile likelihood confidence intervals. (**B**) Respiratory carbon demands of plankton < 100 μm and mesozooplankton communities in the epipelagic (z_e-150 m, top panel) and hadopelagic (6000 m-seabed, bottom panel) zones from Sites A2 and A4. Note that no zooplankton carbon demands are considered in the *FC* profiles from Sites A1 and A8 (*see* Table S3).

depth, whereas the *FC* built on zooplankton respiration decreased in a power law manner.

Modeled *FC* was positively correlated with surface NPP (Spearman $\rho = 0.94$, *p*-value = 0.016, *see* Fig. 5A). The amount of carbon fluxing out from the bottom of the euphotic zone peaked at Site T3 (Fig. 4A), despite its water column was the narrowest among all stations. In this site, 69.1 mmol C m^{-2} d^{-1} were necessary to satisfy the aforementioned large respiration rates, which were fueled by the highly productive conditions in the sunlit layer (Table 1). More attenuated *FC* were found in the more oligotrophic regions, with *FC* surface values ranging between 7.5 and 12.7 mmol C m^{-2} d^{-1} in Sites A8 and T5, respectively. According to our models, at least 1.6 mmol C m^{-2} d^{-1} (Site A2) and 1.0 mmol C m^{-2} d^{-1} (Site A4) should enter into hadal waters over the trench to meet the pelagic carbon demands in this ultra-deep environment (Table 2). Most of the respiratory carbon needs were attributable to the plankton community < 100 μm (Fig. 4B), with mesozooplankton representing about the 10% of the plankton carbon requirements. This percentage was reduced with

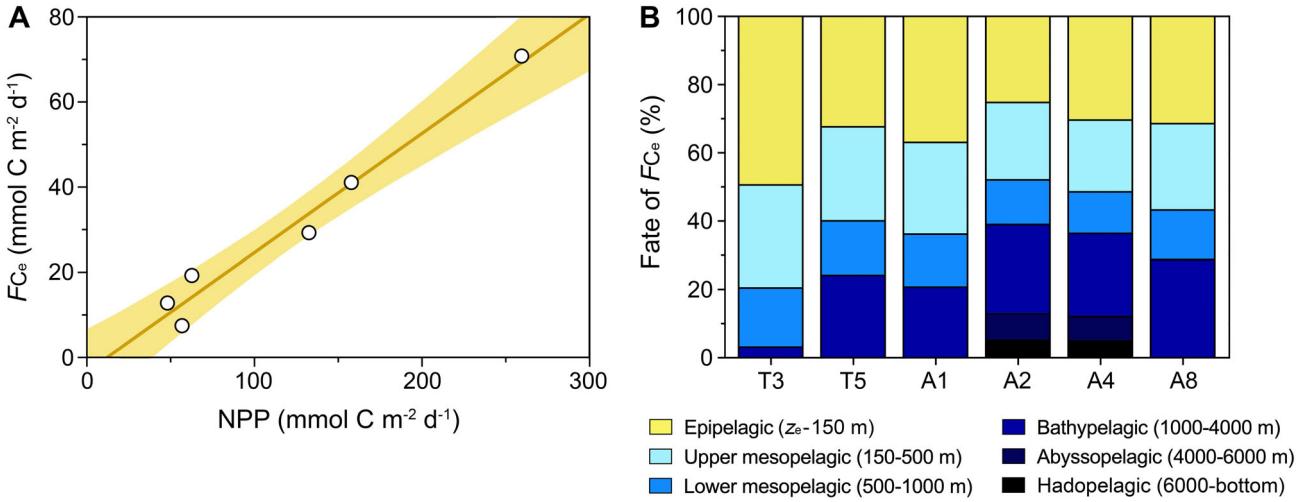

Fig 5. (**A**) Relationship between the respiratory *FC* fluxing out from the euphotic zone (*y*-axis) and the surface NPP (*x*-axis). Light yellow represents the 95% profile likelihood confidence intervals. Both variables where highly correlated according to the linear regression *FCe* = 0.28 NPP – 3.3 (r^2 = 0.969; Spearman ρ = 0.94, *p*-value = 0.016). (**B**) The fate of carbon exported from the euphotic zone (*FCe*) at each station, expressed as percentages. The raw values of the respiratory carbon demand at each zone used to calculate the fate of carbon are given in Table 2.

Table 2. Respiratory carbon demands of the plankton community integrated at each depth zone. Calculations come from the difference in the *FC* values between the upper and the lower depth limits of each realm.

	Respiratory carbon demand (mmol C m^{-2} d^{-1})					
	Epipelagic (z_e–150 m)	**Upper mesopelagic (150–500 m)**	**Lower mesopelagic (500–1000 m)**	**Bathypelagic (1000–4000 m)**	**Abyssopelagic (4000–6000 m)**	**Hadopelagic (6000 m-bottom)**
Site T3	34.0	20.8	12.0	2.3	–	–
Site T5	4.1	3.5	2.0	3.1	–	–
Site A1	15.1	11.0	6.4	8.6	–	–
Site A2	7.3	6.7	3.8	7.7	2.3	1.6
Site A4	5.8	4.1	2.4	4.7	1.4	1.0
Site A8	2.4	1.9	1.1	2.2	–	–

increasing the water depth. The relative importance of size to total carbon demand at different depth layers is shown in Fig. 6. The higher the slope of the regressions, the lower the contribution of the large sizes to remineralization. On this basis, there was a clear trend whereby the large sizes diminished their role as recyclers of organic carbon with increasing depth. Conversely, the largest size class of zooplankton did not fit this pattern, but they gained relative significance in deeper layers instead. It should be noted that the smallest size-class was likely dominated by organisms at the lower-end of the size-range (i.e., prokaryotes) so there may be a potential bias affecting the *b*-values (slopes); nevertheless, this possible artifact would equally impact all regressions, so the pattern of increasing the slope with increasing water depth will remain unaltered.

From a biogeochemical perspective, most of the organic carbon required below the euphotic zone (FC_e) was respired within the upper 1000 m of the water column (Fig. 5B). On average, about 35% of the FC_e was consumed in the epipelagic zone, i.e., between 2.4 and 34.0 mmol C m^{-2} d^{-1} depending on the site (Table 2), values that did not differ significantly from those estimated for the mesopelagic (3.0–32.8 mmol C m^{-2} d^{-1}; Student's *t*-test, *p*-value = 0.145). Nevertheless, as much as ~ 20%–40% of the FC_e (from 2.2 to 10.7 mmol C m^{-2} d^{-1}) occurred below the bathypelagic boundary, the depth at which the effective carbon sequestration occurs. In comparison, a lesser proportion of carbon was needed in the abyssopelagic and hadopelagic zones (~ 12% and 5%, respectively), still non-negligible figures considering the great depths.

POC flux in the water column

Results for the Lutz and GBC14 POC flux models are shown in Tables S5, S6, and summarized in Table 3. Despite the

Table 3. Comparison between the respiratory *FC* in the water column and the POC flux estimated through various approaches. POC flux estimates based on Lutz and GBC14 models consider NPP values calculated from both VGPM and CbPM. Data for all individual sites are available in Tables S5, S6. The standard deviations are given in parentheses when available. z_e stands for the euphotic zone depth. The depths for the abyssal plain are set according to the sediment traps (STs) deployed by Hebbeln et al. (2000). *n.d.* stands for no-data. The minimum export flux required to meet the respiratory carbon demands below the z_e (i.e., the theoretical *e*-ratios estimated from *FC*) and the actual *e*-ratios calculated from 1-D POC flux models are also presented.

	POC flux (mmol C m^{-2} d^{-1})					
Continental slope	**z_e**	**500 m**	**1000 m**	**2000 m**	***e*-ratio (%)**	**Reference**
Respiratory *FC*	41.0 (±28.2)	11.5 (±5.5)	5.9 (±3.9)	1.7 (±0.8)	26.3 (±0.3)	This study
Modeled POC flux						
GBC14 model (VGPM)	12.4 (±7.0)	3.8 (±2.2)	2.4 (±1.4)	1.5 (±0.9)	9.0 (±0.1)	This study
GBC14 model (CbPM)	8.4 (±4.0)	2.6 (±1.2)	1.6 (±0.8)	1.0 (±0.5)	8.6 (±0.5)	This study
Lutz model (VGPM)	7.6 (±4.9)	5.1 (±3.2)	3.4 (±2.1)	1.1 (±0.1)	5.3 (±0.5)	This study
Lutz model (CbPM)	4.8 (±2.1)	3.3 (±1.4)	2.3 (±1.0)	1.1 (±0.5)	4.9 (±0.1)	This study
Martin's curve*	11.0 (±2.6)	4.8 (±1.1)	3.6 (±0.8)	2.7 (±0.6)	5.6 (±1.9)	González et al. 1998

	POC flux (mmol C m^{-2} d^{-1})						
Atacama trench	**z_e**	**500 m**	**1000 m**	**4000 m**	**6000 m**	***e*-ratio (%)**	**Reference**
Respiratory *FC*	24.4 (±7.1)	12.5 (±4.2)	9.3 (±3.1)	3.1 (±1.0)	1.3 (±0.4)	26.4 (±6.1)	This study
Modeled POC flux							
GBC14 model (VGPM)	7.2 (±0.2)	2.2 (±0.1)	1.4 (±0.0)	0.6 (±0.0)	0.5 (±0.0)	9.1 (±0.1)	This study
GBC14 model (CbPM)	4.5 (±0.4)	1.4 (±0.1)	0.9 (±0.1)	0.4 (±0.0)	0.4 (±0.0)	7.6 (±0.1)	This study
Lutz model (VGPM)	3.8 (±0.3)	2.6 (±0.2)	1.8 (±0.1)	0.4 (±0.0)	0.3 (±0.0)	4.8 (±0.3)	This study
Lutz model (CbPM)	2.7 (±0.3)	1.9 (±0.3)	1.3 (±0.1)	0.3 (±0.0)	0.2 (±0.0)	4.7 (±0.1)	This study
Martin's curve†	7.7 (±1.2)	3.2 (±0.5)	2.3 (±0.4)	1.1 (±0.2)	0.9 (±0.1)	7.9 (±5.4)	González et al. 1998

	POC flux (mmol C m^{-2} d^{-1})						
Abyssal plain	**z_e**	**500 m**	**1000 m**	**2300 m**	**3700 m**	***e*-ratio (%)**	**Reference**
Respiratory *FC*	7.6	3.3	2.2	0.9	0.1	13.2	This study
Modeled POC flux							
GBC14 model (VGPM)	6.1	1.9	1.2	0.7	0.5	8.9	This study
GBC14 model (CbPM)	3.8	1.2	0.7	0.4	0.3	7.3	This study
Lutz model (VGPM)	3.2	2.2	1.5	0.7	0.4	4.7	This study
Lutz model (CbPM)	2.3	1.6	1.2	0.5	0.3	4.5	This study
Martin's curve‡	4.5 (±0.3)	1.6 (±0.1)	0.9 (±0.1)	0.5 (±0.0)	0.3 (±0.0)	10.3 (±7.1)	González et al. 1998
STs record	n.d.	n.d.	n.d.	1.1 (±0.4)	0.7 (±0.3)	n.d.	Hebbeln et al. 2000

*Calculated from free-drifting STs deployed between 65 and 300 in the coastal region off Antofagasta: POC flux = 11.47 $(z/65)^{-0.43}$.
†Calculated from free-drifting STs deployed between 65 and 300 in onshore and offshore waters off Antofagasta: POC flux = 9.58 $(z/65)^{-0.53}$.
‡Calculated from free-drifting STs deployed between 65 and 300 in open ocean waters off Antofagasta: POC flux = 8.01 $(z/65)^{-0.80}$.

differences in the models and uncertainties in the fitted parameters, both provided similar values that were comparable to those calculated from in situ sediment traps and derived models (Table 3). However, the GBC14 model consistently led to higher POC export flux estimates at the base of the euphotic zone than the Lutz model (Fig. S1).

Discussion

Based on unique vertical profiles of plankton < 100 μm and mesozooplankton respiration, we present one of the very few assessments of hadopelagic carbon demands in a first attempt to model the minimum carbon flux required throughout the extraordinarily deep waters of the Atacama Trench region. Our results indicate that the water column metabolism over the trench is largely shaped by the surface productivity (Spearman $\rho = 0.94$, p-value = 0.016). Considering the estimated sedimentation rates at different depths (Table 3), it may be presumed that the rain of POC would suffice much of the respiratory needs measured in the ultra-deep waters from the eastern South Pacific. Paradoxically, a great imbalance in the carbon budget was detected in the upper water column

when comparing our respiratory *FC* and estimates of POC flux as illustrated in Fig. 7.

Carbon losses from plankton community respiration

The Peru-Chile coastal current off northern Chile is characterized by a weak seasonality, with wind-driven upwelling events maintaining a high biological productivity all year round (Strub et al. 1998). Such productive conditions, which may be extended farther offshore via mesoscale processes, generate a permanent and well-developed OMZ in the region that has strong biogeochemical implications, as the oxygen-deficient waters constrain the plankton community to a narrow shallower oxygenated layer of intense remineralization (Pantoja et al. 2004). This vertical zonation impacts the carbon flux attenuation and, ultimately, the efficiency of the biological pump as discussed below. In our study, all these features resulted in high community respiration rates within the upper 30 m (ranging between 19.7–37.1 mmol C m^{-2} d^{-1} in plankton < 100 μm and 2.3–18.8 mmol C m^{-2} d^{-1} in mesozooplankton) that were comparable to those previously reported for the surface mixed layer of the region (e.g., Eissler and Quiñones 1999; Donoso and Escribano 2014). These remineralization rates, which represent one of the greatest in the world oceans, suffered a sharp decline by more than an order of magnitude in and below the OMZ (Figs. 2, 3). This was partially explained by the lower plankton biomass, but attending to the depressed respiration rates after protein standardization, other factors should also play a role. Strikingly, the biomass-specific zooplankton respiration peaked to ~ 0.5 μmol C mg $protein^{-1}$ h^{-1} in the upper oxygen-depleted zone (90–150 m, Fig. 3C). Increasing the mitochondrial density in the cells, and therefore their enzyme load, may help to offset the effect of low oxygen (Childress and Seibel 1998), enabling effective removal of the little oxygen available from the seawater.

Nevertheless, the plankton metabolic response in the vertical domain is regulated by a combination of factors. In addition to low-oxygen levels, organisms living in the deep ocean are exposed to cold temperatures, food shortage and darkness, which usually results in a reduction in locomotory abilities (Childress 1995) and in larger body sizes (Timofeev 2001). Among all, the temperature effect on the respiratory metabolism is probably the best known and the most important. Like any other chemical reaction, respiration is related to temperature through an Arrhenius relationship, with Q_{10} coefficient values between 3.0 and 3.6 for the mesopelagic zone (Mazuecos et al. 2015). Accordingly, the temperature may be responsible for about 5-fold decrease in the plankton respiration from the surface temperatures to the hadal ones. Moreover, the more limited access to an energy source (and of poorer quality) will affect the intracellular pool of pyridine nucleotides, the substrates that fuel respiration, negatively (Osma et al. 2016). Altogether, these factors explain the low community respiration rates that we observed at depth, which remained fairly constant below the mesopelagic zone. This minor variation in the deep waters further reveals that, even though the extreme hydrostatic pressure poses a biochemical challenge, it appears to have little effect on the community respiration.

On average, the plankton community < 100 μm respired 13.2 (± 8.4) μmol C m^{-3} d^{-1} in the dark waters below 1000 m, which concurs with those rates previously found in other bathypelagic realms (e.g., Baltar et al. 2009); conversely, zooplankton respiration averaged 1.0 (± 0.4) μmol C m^{-3} d^{-1} between 1000 and 5158 m, an order of magnitude lower than that of plankton < 100 μm, yet significantly higher than the only available estimate for ultra-deep bathypelagic zooplankton (Koppelmann et al. 2004). These authors measured zooplankton respiration rates in the bathypelagic zone of the oligotrophic eastern Mediterranean (0.01 μmol C m^{-3} d^{-1}), with extremely low biomass-specific respiration rates at 4250 m (0.003 μmol C mg $protein^{-1}$ h^{-1}). Their values are far below the specific-rates measured in our study (0.06 ± 0.02 μmol C mg $protein^{-1}$ h^{-1}), which are closer to those provided by Ikeda (2011) for bathy- and abyssopelagic zooplankton in the similarly productive western subartic Pacific (0.02 μmol C mg $protein^{-1}$ h^{-1}). This means that, aside from temperature effects, the deep-sea metazoa in our region may have a better metabolic fitness, probably due to an increased accessibility to energy-rich sinking particles.

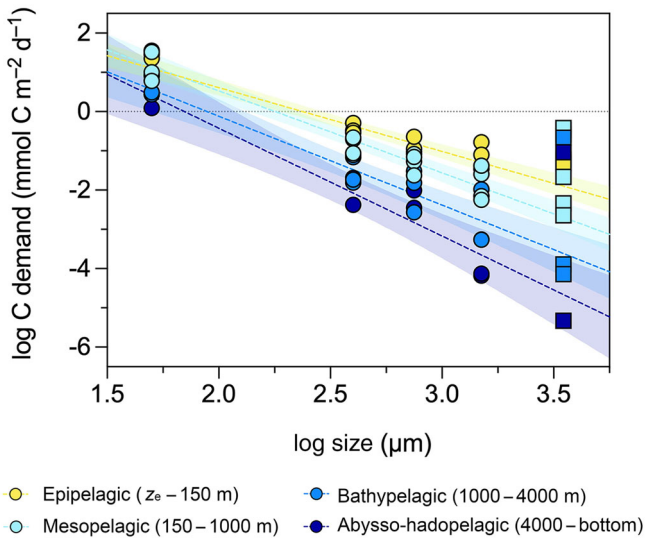

Fig 6. Log–log relationships between respiratory carbon demand (*y*-axis) and size fraction (*x*-axis) in the epipelagic (log $y = -1.63 \log x + 3.8$, $r^2 = 0.937$), mesopelagic (log $y = -2.08 \log x + 4.7$, $r^2 = 0.936$), bathypelagic (log $y = -2.26 \log x + 4.4$, $r^2 = 0.900$), and abysso-hadopelagic (log $y = -2.75 \log x + 5.1$, $r^2 = 0.917$) zones. The sizes considered in the *x*-axis before logarithm transformation correspond to the mid-value of the five aforementioned size-classes. The largest size class (square symbols) is not considered in the linear regressions as it showed a different and more variable pattern in the carbon requirements.

The typically low volumetric rates in the deep ocean are, nevertheless, largely compensated by the extent of this ecosystem, making it a relevant component to consider in the pelagic carbon attenuation. In fact, the respiratory carbon demands integrated through the bathy-, abysso-, and hadopelagic realms over the trench (9.3 ± 3.1 mmol C m^{-2} d^{-1}) were higher than those in the mesopelagic (8.5 ± 2.9 mmol C m^{-2} d^{-1}) and epipelagic (6.6 ± 1.1 mmol C m^{-2} d^{-1}) zones (Table 2). The contribution of each component of the plankton community to the total carbon losses via respiration (Fig. 4B) was consistent with the carbon flow balance given for the coastal waters off Chile (Thiel et al. 2007).

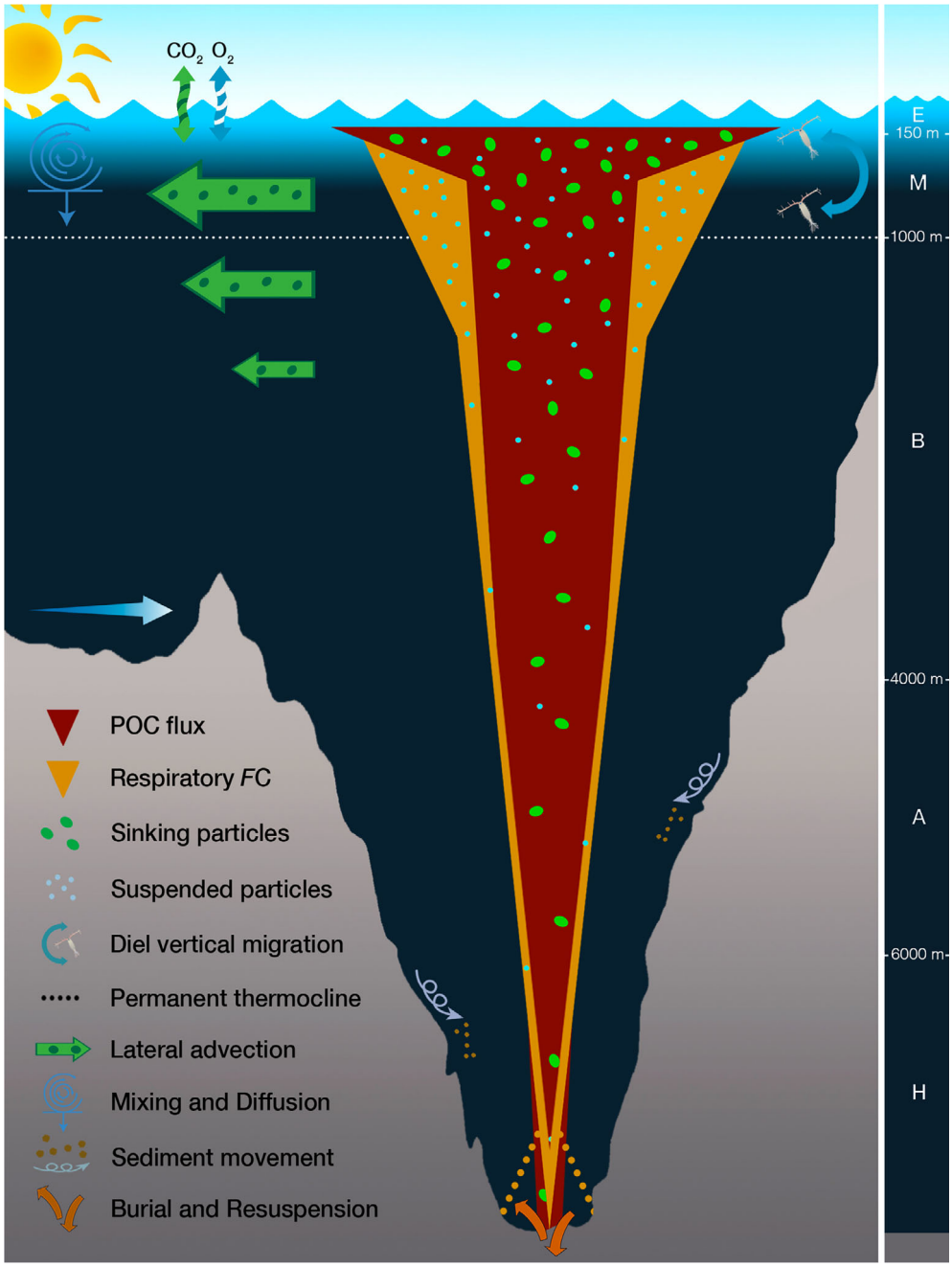

Fig 7. Conceptual scheme illustrating the relationship between the POC flux and the respiratory *FC* attenuation, including some of the processes that may have a role in the carbon budget. The width of each flux symbol represents its magnitude. Wider yellow than red areas (i.e., higher *FC* than POC flux) indicates an apparent carbon deficiency, while the opposite (wider dark red than yellow areas) means carbon surplus. Increased respiration near the bottom (dotted yellow line) is presumably associated to processes occurring in the benthic boundary layer, such as resuspension and sediment movement. The bar in the right side delimits the epipelagic (E), mesopelagic (M), bathypelagic (B), abyssopelagic (A), and hadopelagic (H) depth layers.

Prokaryotes and protists are known to be the main remineralizers in the ocean water columns, with respiratory carbon demands that exceeded those of the larger zooplankton by several fold in our study. The relevance of plankton < 100 μm to the community metabolism increased with water depth (Fig. 6), partially because of the vertical migration that some zooplankters perform during nighttime to the surface (Tutasi and Escribano 2020). However, the largest size class showed a more variable pattern, gaining relative importance in the deep ocean compared to the small mesozooplankton (Fig. 6). The typical trend toward increased body size with increased depth in marine metazoan would also imply an increased ecological role of large organisms such as amphipods at great depths (Timofeev 2001). Unfortunately, the net avoidance capability of these fast swimmers together with the patchiness in their distribution usually lead to the high variability that we found, and to considerable underestimation of their biomass.

Respiratory flux and carbon budget in the deep ocean

Both the export flux and the depth at which the sinking organic material is remineralized determine the ability of the biological pump to sequester carbon in the ocean interior. The ratio of particulate export to primary production at the base of the euphotic zone, the so-called *e*-ratio, is commonly used as a proxy for the export efficiency in marine ecosystems (Buesseler and Boyd 2009). Here, according to the regression slope given in Fig. 5A, at least 28% of what was produced in the sunlit layer should, in an ideal steady-state scenario, flux out of the euphotic zone to meet the heterotrophic carbon demands below that depth. The theoretical *e*-ratio estimated from the *F*C approach decreased toward the open ocean from 26% onshore to 13% in waters over the abyssal plain (Table 3). Increased NPP usually leads to an enhanced transference of organic carbon to deep waters, which in turn maintains an increased plankton biomass and metabolic activities in the water column (Hernández-León et al. 2020). Hence the tight relationship between NPP and *F*C (Fig. 5A). The theoretical e-ratios were, however, somewhat at odds with the actual *e*-ratios assessed from various POC flux models in our study (4.7%–10.3%, Table 3) and with those previously calculated in the region by sediment traps (averaging 7.9 $\pm$ 5.4% according to González et al. 1998). Given the conservative nature of our *F*C modeling approach, there are two potential reasons for the discrepancy between the theoretical and actual *e*-ratios: (1) all 1-D models of POC flux underestimated the *e*-ratios, and (2) the respiratory plankton demands in the water column may not be totally fulfilled by the rain of POC.

Relatively low *e*-ratios in these productive waters are explained by the high remineralization in the surface mixed layer above the OMZ. This was evidenced by the great curvatures of the respiratory power models (Table S2), particularly in those of zooplankton, which resulted in a rapid and effective carbon flux attenuation within the upper water column. Nevertheless, a significant amount of organic material was still exported from the euphotic zone (up to 12.4 $\pm$ 7.0 mmol C m^{-2} d^{-1} in waters over the continental slope). Using ^{234}Th to derive *e*-ratios and transfer efficiencies, Black et al. (2018) already observed a strong coastal biological pump in the eastern South Pacific, but one with a high POC attenuation in the upper ocean. Here, the sinking POC was apparently not enough to sustain the respiratory *F*C calculated at mesopelagic and upper bathypelagic depths (Table 3), so other carbon sources should come into play in these zones to balance the carbon losses. It might also be that the POC flux may have been underestimated to some extent by the 1-D modeling approaches used here. These models have uncertainties associated with satellite data-based products and are highly sensitive to the fitted parameters. Moreover, most of them are based on conical traps that are prone to underestimate flux gradients (Gardner 2000). This was the case of the Lutz et al. (2002) model, which resulted in lower export fluxes than those calculated from the food-web based method of Siegel et al. (2014) (Fig. S1). Nevertheless, despite their inherent uncertainties, both Lutz and GBC14 models compared well with sedimentation rates measured by in situ sediment traps at mesopelagic (González et al. 1998; Haskell et al. 2013) and bathypelagic depths (Hebbeln et al. 2000). Here, we considered models built on different sets of assumptions, various NPP estimates and attenuation coefficients to provide reliable ranges of POC flux (Table 3 and Supp. Tables S5, S6), and yet none was able to meet the respiratory *F*C through the mesopelagic zone. This discrepancy between *F*C and POC flux could also come from an overestimation of actual respiration by the R/ETS ratios, but given that we applied conservative values, it does not seem to explain such an imbalance either. The factor that relates both rates in plankton communities usually ranges between 0.5 and the theoretical maximum value of 1.0 (Arístegui and Montero 1995; Hernández-León and Gómez 1996, among others). Our R/ETS ratios fall at the lower end of this range and are lower than those previously applied in the same marine area by González et al. (1998). Therefore, our estimates most likely represent the minimum *F*C, which is indeed supported by recent findings of Hernández-León et al. (2019) who observed significantly more attenuated respiration rates in the mesopelagic when using a R/ETS ratio of 0.5 instead of other proxies such as the Q_{10} or any of Ikeda's equations (Ikeda 2014). Assuming denitrification processes in the hypoxic core and applying a respiratory quotient lower than the commonly used 0.97 (Steinberg and Landry 2017), we further prevented overestimation of *F*C.

Apparent imbalances in the ocean carbon cycle have long been a source of controversy, with only few attempts in the literature being successful in closing the budget (Giering et al. 2014). In most cases, deep-sea plankton respiration exceeds the amount of carbon supplied by gravitational sinking (e.g., Steinberg et al. 2008; Baltar et al. 2009), similar to what we found down to the bathypelagic zone when

comparing POC flux values to our *F*C models (Table 3). The complex interplay between carbon sinks and sources within the dimly lit waters of the mesopelagic zone are still not well understood, but growing evidence points to a major role of small suspended particles in sustaining the excess of respiration throughout the twilight zone (Riley et al. 2012). Slow sinking and suspended particles are known to be poorly quantified by sediment traps (Gardner 2000) and consequently, they are greatly underestimated by most biogeochemical models. These small particles originate from the fragmentation of larger ones, a mechanical process primarily led by zooplankton grazing (Mayor et al. 2014). The concentration of suspended particles is therefore expected to be high in those depths of intense zooplankton remineralization, namely in the epipelagic and upper mesopelagic zones (Fig. 3B), from where they can be either laterally advected by mesoscale features or transported to bathypelagic depths by mixing processes. It is precisely around the mesopelagic/bathypelagic boundary where they seem to be crucial to balance the cycle as illustrated in the conceptual scheme (Fig. 7). The long residence times in the water column of these small organic particles may help sustaining respiration over time, increasing their likelihood to be remineralized before reaching the abyss. Sources of carbon other than the gravitational settling flux and the suspended particles originated from the disaggregation of the sinking material will additionally contribute a proportion of the subsurface respiration by injecting organic matter to depth (Boyd et al. 2019). For instance, vertically migrating zooplankton may actively transport 5.9 mmol C m^{-2} d^{-1} to the mesopelagic (Tutasi and Escribano 2020) which, together with the downward mixing and diffusion of dissolved organic carbon and the lateral inputs of POC advected from the coast (Shen et al. 2020), will help to reconcile the unbalanced carbon cycle. Unfortunately, quantifying the relative contribution of all these physical and biological processes that make up the biological pump is outside the scope of this research.

Strikingly, the carbon imbalance in the upper layers was reduced or even reversed at a given depth between the bathypelagic and abyssal realms (Table 3). Recent studies have demonstrated that some, photosynthetically produced, fast sinking particles can escape from remineralization in the twilight zone, and that these are critical to meet the carbon requirements below the bathypelagic (Agustí et al. 2015; Grabowski et al. 2019). Such is the case of diatom aggregates and fecal pellets, which have indeed been found to be the most prominent type of particles contributing to the vertical flux in our region (González et al. 2009). These particles, with sinking velocities over 300 m d^{-1}, could reach ultra-deep waters in a matter of weeks, as reflected by the synchronicity of the flux patterns in two traps vertically-separated from one another by 1400 m in these same lower bathypelagic waters (Hebbeln et al. 2000). The steady-state assumption may thus be valid in an ultra-deep ocean characterized by rapidly sinking particles and low lateral advection, a condition that would buffer the imbalance between respiratory carbon demand and supply typically found in the non-steady state upper ocean (Giering et al. 2017).

Implications for hadal biogeochemistry

The findings here, combined with results from complementary studies in the Atacama Trench, suggest a close link between surface productivity and hadal ecosystem processes. Despite the lack of respiratory data from other trenches to compare with, there have been found higher prokaryotic abundances in the hadopelagic zone of the Atacama Trench than in hadal realms underlying less productive water columns (Schauberger et al. 2021). Given that prokaryotes are an important component of the plankton $< 100\ \mu$m, and that these were responsible for most of the respiratory carbon demands measured here (Fig. 5), it seems reasonable to expect a similar spatial pattern for the community respiration than that observed in the cell abundances. The characteristically low *e*-ratios estimated in the region may be compensated by efficient transport mechanisms that would rapidly inject some fresh photosynthetic material into the hadal realm. Although limited, the amount of biogenic matter reaching the deep-sea was enough to sustain respiration in the lower bathypelagic waters of shallower nearby sites, yet it did not totally suffice the carbon needs within the trench (Table 3). The difference between carbon demand and supply in hadal waters was, in any case, much lower than the one detected in upper layers, and was indeed lower than the cumulative error associated with each estimation. It must further be noted that the 1-D vertical POC flux models such as those applied in this study are prone to underestimate the sinking flux at great depths because they do not consider the "source funnel" sensu Siegel et al. (2008), which implies that the particulate material at depth come from a larger surface area. The "source funnel" closely depends both on the particle size and water depth and therefore, in a marine environment dominated by fast sinking particles, it will be particularly relevant in the deep waters within the actual trench. This would explain why the sediment traps collected more POC at bathypelagic depths than that predicted from any of the POC flux models (Table 3). Moreover, additional carbon inputs coming from resuspension and sediment movement along the trench slope, especially within the benthic boundary layer, would also help to meet some of the metabolic demands. The downslope sediment transport into the trench basin is indeed a common feature to all marine trenches, so it would hardly explain, by itself, ecological differences among them. This study ultimately aims to be a first-approximation to hadopelagic biogeochemistry through a modeling approach, and so the relative contribution of each carbon source to the total POC pool in hadal waters still remains unresolved. We encourage further research to quantify and characterize the sinking particles reaching the trench waters; the use of more direct and standardized

approaches like sediment traps above and within the benthic boundary layer of the trench would be key for future investigations to test the hypothesis that fresh, energy-replete, large sinking particles are effectively sustaining life in this ultra-deep marine environment.

References

Agustí, S., J. I. González-Gordillo, D. Vaqué, M. Estrada, M. I. Cerezo, G. Salazar, J. M. Gasol, and C. M. Duarte. 2015. Ubiquitous healthy diatoms in the deep sea confirm deep carbon injection by the biological pump. Nat. Commun. **6**: 1–8. doi:10.1038/ncomms8608

Arístegui, J., and M. F. Montero. 1995. The relationship between community respiration and ETS activity in the ocean. J. Plankton Res. **17**: 1563–1571. doi:10.1093/plankt/17.7.1563

Baltar, F., J. Arístegui, J. M. Gasol, E. Sintes, and G. J. Herndl. 2009. Evidence of prokaryotic metabolism on suspended particulate organic matter in the dark waters of the subtropical North Atlantic. Limnol. Oceanogr. **54**: 182–193. doi:10.4319/lo.2009.54.1.0182

Behrenfeld, M. J., and P. G. Falkowski. 1997. Photosynthetic rates derived from satellite-based chlorophyll concentration. Limnol. Oceanogr. **42**: 1–20. doi:10.4319/lo.1997.42.1.0001

Black, E. E., K. O. Buesseler, S. M. Pike, and P. J. Lam. 2018. ^{234}Th as a tracer of particulate export and remineralization in the southeastern tropical Pacific. Mar. Chem. **201**: 35–50. doi:10.1016/j.marchem.2017.06.009

Blankenship, L. E., A. A. Yayanos, D. B. Cadien, and L. A. Levin. 2006. Vertical zonation patterns of scavenging amphipods from the Hadal zone of the Tonga and Kermadec trenches. Deep-Sea Res. I Oceanogr. Res. Pap. **53**: 48–61. doi:10.1016/j.dsr.2005.09.006

Boyd, P. W., H. Claustre, M. Levy, D. A. Siegel, and T. Weber. 2019. Multi-faceted particle pumps drive carbon sequestration in the ocean. Nature **568**: 327–335. doi:10.1038/s41586-019-1098-2

Buesseler, K. O. 1998. The decoupling of production and particulate export in the sea surface. Global Biogeochem. Cycles **12**: 297–310. doi:10.1029/97GB03366

Buesseler, K. O., and P. W. Boyd. 2009. Shedding light on processes that control particle export and flux attenuation in the twilight zone of the open ocean. Limnol. Oceanogr. **54**: 1210–1232. doi:10.4319/lo.2009.54.4.1210

Buesseler, K. O., P. W. Boyd, E. E. Black, and D. A. Siegel. 2020. Metrics that matter for assessing the ocean biological carbon pump. Proc. Natl. Acad. Sci. USA **117**: 1–9. doi:10.1073/pnas.1918114117

Cadman, E., R. J. Bostwick, and J. Eichberg. 1979. Determination of protein by a modified Lowry procedure in the presence of some commonly used detergents. Anal. Biochem. **96**: 21–23. doi:10.1016/0003-2697(79)90548-7

Childress, J. J. 1995. Are there physiological and biochemical adaptations of metabolismin deep-sea animals? Trends Ecol. Evol. **10**: 30–36. doi:10.1016/S0169-5347(00)88957-0

Childress, J. J., and B. A. Seibel. 1998. Life at stable low oxygen levels: Adaptations of animals to oceanic oxygen minimum layers. J. Exp. Biol. **201**: 1223–1232.

Danovaro, R., C. Gambi, and N. Della Croce. 2002. Meiofauna hotspot in the Atacama Trench, eastern South Pacific Ocean. Deep-Sea Res. I Oceanogr. Res. Pap. **49**: 843–857. doi:10.1016/S0967-0637(01)00084-X

De La Rocha, C. L., and U. Passow. 2007. Factors influencing the sinking of POC and the efficiency of the biological carbon pump. Deep-Sea Res. II Top. Stud. Oceanogr. **54**: 639–658. doi:10.1016/j.dsr2.2007.01.004

Donoso, K., and R. Escribano. 2014. Mass-specific respiration of mesozooplankton and its role in the maintenance of an oxygen-deficient ecological barrier (BEDOX) in the upwelling zone off Chile upon presence of a shallow oxygen minimum zone. J. Mar. Syst. **129**: 166–177. doi:10.1016/j.jmarsys.2013.05.011

Eissler, Y., and R. A. Quiñones. 1999. Microplanktonic respiration off northern Chile during El Niño 1997–1998. J. Plankton Res. **21**: 2263–2283. doi:10.1093/plankt/21.12.2263

Fernández-Urruzola, I., N. Osma, T. T. Packard, M. Gómez, and L. Postel. 2014. Distribution of zooplankton biomass and potential metabolic activities across the northern Benguela upwelling system. J. Mar. Syst. **140**: 138–149. doi:10.1016/j.jmarsys.2014.05.009

Fujii, T., N. M. Kilgallen, A. A. Rowden, and A. J. Jamieson. 2013. Deep-sea amphipod community structure across abyssal to hadal depths in the Peru-Chile and Kermadec trenches. Mar. Ecol. Prog. Ser. **492**: 125–138. doi:10.3354/meps10489

Gardner, W. D. 2000. Sediment trap sampling in surface waters, p. 240–284. *In* The changing ocean carbon cycle: A midterm synthesis of the Joint Global Ocean Flux Study. Cambridge Univ. Press.

Giering, S. L. C., and others. 2014. Reconciliation of the carbon budget in the ocean's twilight zone. Nature **507**: 1–17. doi:10.1038/nature13123

Giering, S. L. C., R. Sanders, A. P. Martin, S. A. Henson, J. S. Riley, C. M. Marsay, and D. G. Johns. 2017. Particle flux in the oceans: Challenging the steady state assumption. Global Biogeochem. Cycles **31**: 159–171. doi:10.1002/2016GB005424

González, H. E., and others. 1998. Producción primaria y su destino en la trama trófica pelágica y océano profundo en la zona norte de la Corriente de Humboldt (23 °S): Posibles efectos del evento El Niño, 1997–1998 en Chile. Rev. Chil. His. Nat. **71**: 429–458.

González, H. E., G. Daneri, J. L. Iriarte, B. Yannicelli, E. Menschel, C. Barría, S. Pantoja, and L. Lizárraga. 2009. Carbon fluxes within the epipelagic zone of the Humboldt

current system off Chile: The significance of euphausiids and diatoms as key functional groups for the biological pump. Prog. Oceanogr. **83**: 217–227. doi:10.1016/j.pocean.2009.07.036

Grabowski, E., R. M. Letelier, E. A. Laws, and D. M. Karl. 2019. Coupling carbon and energy fluxes in the North Pacific subtropical gyre. Nat. Commun. **10**: 1895. doi:10.1038/s41467-019-09772-z

Haskell, W. Z., W. M. Berelson, D. E. Hammond, and D. G. Capone. 2013. Particle sinking dynamics and POC fluxes in the eastern tropical South Pacific based on ^{234}Th budgets and sediment trap deployments. Deep-Sea Res. I **81**: 1–13. doi:10.1016/j.dsr.2013.07.001

Hebbeln, D., M. Marchant, and G. Wefer. 2000. Seasonal variations of the particle flux in the Peru-Chile current at 30° S under "normal" and El Niño conditions. Deep-Sea Res. II **47**: 2101–2128.

Hernández-León, S., and M. Gómez. 1996. Factors affecting the respiration/ETS ratio in marine zooplankton. J. Plankton Res. **18**: 239–255. doi:10.1093/plankt/18.2.239

Hernández-León, S., S. Calles, and M. L. F. de Puelles. 2019. The estimation of metabolism in the mesopelagic zone: Disentangling deep-sea zooplankton respiration. Prog. Oceanogr. **178**: 102163. doi:10.1016/j.pocean.2019.102163

Hernández-León, S., and others. 2020. Large deep-sea zooplankton biomass mirrors primary production in the global ocean. Nat. Commun. **1–8**: 6048. doi:10.1038/s41467-020-19875-7

Ikeda, T. 2011. Metabolic activity of pelagic copepods from 5,000 to 7,000 m depth of the western subarctic Pacific, as inferred from electron transfer system (ETS) activity. J. Oceanogr. **67**: 785–790. doi:10.1007/s10872-011-0067-7

Ikeda, T. 2014. Respiration and ammonia excretion by marine metazooplankton taxa: Synthesis toward a global-bathymetric model. Mar. Biol. **1–14**: 2753–2766. doi:10.1007/s00227-014-2540-5

Jamieson, A. 2018. A contemporary perspective on hadal science. Deep-Sea Res. II Top. Stud. Oceanogr. **155**: 4–10. doi:10.1016/j.dsr2.2018.01.005

Kenner, R. A., and S. I. Ahmed. 1975. Measurements of electron transport activities in marine phytoplankton. Mar. Biol. **33**: 119–127.

Koppelmann, R., H. Weikert, C. Halsband-Lenk, and T. Jennerjahn. 2004. Mesozooplankton community respiration and its relation to particle flux in the oligotrophic eastern Mediterranean. Global Biogeochem. Cycles **18**: GB1039. doi:10.1029/2003GB002121

Leduc, D., A. A. Rowden, R. N. Glud, F. Wenzhöfer, H. Kitazato, and M. R. Clark. 2016. Comparison between infaunal communities of the deep floor and edge of the Tonga trench: Possible effects of differences in organic matter supply. Deep-Sea Res. I **116**: 264–275. doi:10.1016/j.dsr.2015.11.003

Levin, L. A., and N. L. Bris. 2015. The deep ocean under climate change. Science **350**: 766–768. doi:10.1126/science.aad0126

Lutz, M. J., R. B. Dunbar, and K. Caldeira. 2002. Regional variability in the vertical flux of particulate organic carbon in the ocean interior. Global Biogeochem. Cycles **16**: 1037–1055. doi:10.1029/2000GB001383

Maldonado, F., T. T. Packard, and M. Gómez. 2012. Understanding tetrazolium reduction and the importance of substrates in measuring respiratory electron transport activity. J. Exp. Mar. Biol. Ecol. **434-435**: 110–118. doi:10.1016/j.jembe.2012.08.010

Marsay, C. M., R. J. Sanders, S. A. Henson, K. Pabortsava, E. P. Achterberg, and R. S. Lampitt. 2015. Attenuation of sinking particulate organic carbon flux through the mesopelagic ocean. Proc. Natl. Acad. Sci. USA **112**: 1089–1094. doi:10.1073/pnas.1415311112

Martin, J. H., G. A. Knauer, D. M. Karl, and W. W. Broenkow. 1987. VERTEX: Carbon cycling in the northeast Pacific. Deep-Sea Res. **34**: 267–285.

Mayor, D. J., R. Sanders, S. L. C. Giering, and T. R. Anderson. 2014. Microbial gardening in the ocean's twilight zone: Detritivorous metazoans benefit from fragmenting, rather than ingesting, sinking detritus. Bioessays **36**: 1132–1137. doi:10.1002/bies.201400100

Mazuecos, I. P., E. Vázquez-Dominguez, E. Ortega-Retuerta, J. M. Gasol, and I. Reche. 2015. Temperature control of microbial respiration and growth efficiency in the mesopelagic zone of the South Atlantic and Indian oceans. Deep-Sea Res. Part I: Oceanogr. Res. Pap. **95**: 131–138. doi:10.1016/j.dsr.2014.10.014

Nunoura, T., and others. 2015. Hadal biosphere: Insight into the microbial ecosystem in the deepest ocean on Earth. Proc. Natl. Acad. Sci. USA **112**: E1230–E1236. doi:10.1073/pnas.1421816112

Osma, N., I. Fernández-Urruzola, T. T. Packard, L. Postel, M. Gómez, and F. Pollehne. 2014. Short-term patterns of vertical particle flux in northern Benguela: A comparison between sinking POC and respiratory carbon consumption. J. Mar. Syst. **140**: 150–162. doi:10.1016/j.jmarsys.2014.01.004

Osma, N., I. Fernández-Urruzola, M. Gómez, S. Montesdeoca-Esponda, and T. T. Packard. 2016. Predicting in vivo oxygen consumption rate from ETS activity and bisubstrate enzyme kinetics in cultured marine zooplankton. Mar. Biol. **163**: 1–14. doi:10.1007/s00227-016-2923-x

Owens, T., and F. D. King. 1975. The measurement of respiratory electron transport system activity in marine zooplankton. Mar. Biol. **30**: 27–36.

Packard, T. T., A. Devol, and F. D. King. 1975. The effect of temperature on the respiratory electron transport system in marine plankton. Deep-Sea Res. **22**: 237–249. doi:10.1016/0011-7471(75)90029-7

Packard, T. T., N. Osma, I. Fernández-Urruzola, L. A. Codispoti, J. P. Christensen, and M. Gómez. 2015. Peru upwelling plankton respiration: Calculations of carbon flux, nutrient retention efficiency, and heterotrophic energy production. Biogeosciences **12**: 2641–2654. doi:10.5194/bg-12-2641-2015

Pantoja, S., J. Sepúlveda, and H. E. González. 2004. Decomposition of sinking proteinaceous material during fall in the oxygen minimum zone off northern Chile. Deep-Sea Res. I Oceanogr. Res. Pap. **51**: 55–70. doi:10.1016/j.dsr.2003.09.005

Riley, J. S., R. Sanders, C. Marsay, F. A. C. Le Moigne, E. P. Achterberg, and A. J. Poulton. 2012. The relative contribution of fast and slow sinking particles to ocean carbon export. Global Biogeochem. Cycles **26**: GB1026. doi:10.1029/2011GB004085

Schauberger, C., and others. 2021. Spatial variability of prokaryotic and viral abundances in the Kermadec and Atacama trench regions. Limnol. Oceanogr. **9999**: 1–15. doi:10.1002/lno.11711

Shen, J., and others. 2020. Laterally transported particles from margins serve as a major carbon and energy source for Dark Ocean ecosystems. Geophys. Res. Lett. **47**: 227–212. doi:10.1029/2020GL088971

Siegel, D. A., E. Fields, and K. O. Buesseler. 2008. A bottom-up view of the biological pump: Modeling source funnels above ocean sediment traps. Deep-Sea Res. I **55**: 108–127. doi:10.1016/j.dsr.2007.10.006

Siegel, D. A., K. O. Buesseler, S. C. Doney, S. F. Sailley, M. J. Behrenfeld, and P. W. Boyd. 2014. Global assessment of ocean carbon export by combining satellite observations and food-web models. Global Biogeochem. Cycles **28**: 181–196. doi:10.1002/2013GB004743

Smith, C. R., F. C. De Leo, A. F. Bernardino, A. K. Sweetman, and P. M. Arbizu. 2008. Abyssal food limitation, ecosystem structure and climate change. Trends Ecol. Evol. **23**: 518–528. doi:10.1016/j.tree.2008.05.002

Steinberg, D. K., and M. R. Landry. 2017. Zooplankton and the ocean carbon cycle. Ann. Rev. Mar. Sci. **9**: 413–444. doi:10.1146/annurev-marine-010814-015924

Steinberg, D. K., B. A. S. Van Mooy, K. O. Buesseler, P. W. Boyd, T. Kobari, and D. M. Karl. 2008. Bacterial vs. zooplankton control of sinking particle flux in the ocean's twilight zone. Limnol. Oceanogr. **53**: 1327–1338. doi:10.4319/lo.2008.53.4.1327

Strub, T. P., J. M. Mesías, V. Montecino, J. Rutllant, and S. Salinas. 1998. Coastal Ocean circulation off western South America, p. 273–313. *In* A. R. Robinson and K. H. Brink [eds.], The sea. The Global Coastal Ocean. First Workshop on Coastal Ocean Advanced Science and Technology Studies (COASTS) IOC, Liege, vol. 2. John Wiley & Sons, Inc.

Suess, E. 1980. Particulate organic carbon flux in the oceans-surface productivity and oxygen utilization. Nature **288**: 260–263.

Takahashi, T., W. S. Broecker, and S. Langer. 1985. Redfield ratio based on chemical data from isopycnal surfaces. J. Geophys. Res. **90**: 6907–6924. doi:10.1029/JC090iC04p06907

Thiel, M., and others. 2007. The Humbold current system of northern and Central Chile. Oceanogr. Mar. Biol. **45**: 195–344.

Timofeev, S. F. 2001. Bergmann's principle and deep-water gigantism in marine crustaceans. Biol. Bull. **28**: 646–650. doi:10.1023/A:1012336823275

Tutasi, P., and R. Escribano. 2020. Zooplankton diel vertical migration and downward C flux into the oxygen minimum zone in the highly productive upwelling region off northern Chile. Biogeosciences **17**: 455–473. doi:10.5194/bg-17-455-2020

Tyler, P. A. 2003. Ecosystems of the deep oceans, Ist ed. Elsevier.

Ulloa, O., D. E. Canfield, E. F. DeLong, R. M. Letelier, and F. J. Stewart. 2012. Microbial oceanography of anoxic oxygen minimum zones. Proc. Natl. Acad. Sci. USA **109**: 15996–16003. doi:10.1073/pnas.1205009109

Westberry, T., M. J. Behrenfeld, D. A. Siegel, and E. Boss. 2008. Carbon-based primary productivity modeling with vertically resolved photoacclimation. Global Biogeochem. Cycles **22**: GB2024. doi:10.1029/2007GB003078

Acknowledgments

We would like to thank the captains, crews and scientific personnel that participated in the LowpHox II and SO260 cruises, particularly to D. Toledo for his valuable technical assistance at sea. We are also grateful to N.A. Osma, E. Flores and two anonymous reviewers for providing important insights on the manuscript. This work was funded by the Chilean Agency for Research and Development (grants FONDECYT 3180352 to IFU and AUB17002 to W.S.) and the Millennium Science Initiative-ANID Program (grant ICN12_019-IMO). The MOCNESS was provided by FONDEQUIP grant EQM 140029. Additional support was received from the European Research Council (Hades-ERC, grant agreement number 669947 awarded to R.G.), by the Danish National Research Foundation through the Danish Center for Hadal Research (grant DNRF145) and by the Max Planck Society. The ship time for RV *Sonne* was provided by BMBF, Germany.

Conflict of Interest

None declared.

Submitted 23 October 2020
Revised 16 March 2021
Accepted 22 May 2021

Associate editor: David Antoine